Spontaneous emission spectrum from a V-type artificial atom in a strong-coupling regime: Dark lines and line narrowing

Yiying Yan [*]

Department of Physics, School of Science, Zhejiang University of Science and Technology, Hangzhou 310023, China

We employ a time-dependent variational approach with the multiple Davydov D_2 ansatz and two approximate analytical methods to study the spontaneous emission of a V-type artificial atom in the strong-coupling regime, where the decay rate of the emitter becomes a considerable fraction of its transition frequencies, and focus on quantum-interference-induced effects. The variational approach is found to be accurate in certain strong-coupling regimes and is used as the benchmark to address the validity of the analytical methods: the rotating-wave approximation (RWA) and the transformed RWA (TRWA). It is found that the TRWA is fairly accurate in the strong-coupling regime where the RWA breaks down. By using the numerical and analytical methods, we illustrate that there are dark lines and line narrowing in the emission spectra in the strong-coupling regime and in a wide accessible range of the emitter parameters. We also illustrate how the emission spectrum is altered by the counter-rotating couplings. The present results offer insights into the experimental observation of the quantum-interference-induced effect in the strong-coupling regime and in the context of artificial atoms.

I. INTRODUCTION

Multilevel emitters have attracted much attention in both theoretical and experimental studies in quantum optics because of quantum interference and coherence. Such effects play a vital role in the emission and absorption processes of multilevel emitters and lead to a variety of interesting phenomena such as electromagnetically induced transparency [1–5], spontaneous emission cancellation [6], and lasing without inversion [7]. On the other hand, the study of the multilevel system reveals also a need for the realization of quantum information processing, which is relevant to quantum gates [8], quantum state transfer [9], quantum entanglement [10], etc.

One of the simplest multilevel systems, the three-level systems have been considered in many works [11–21]. Owing to quantum interference and coherence, the time evolution of the excited-state population is not a simple exponential decay. The emission spectrum exhibits intriguing structures that are absent in the case of a two-level atom, the spectrum of which is a simple Lorentzian line. Zhu *et al.* have shown that there are dark lines and line narrowing in the emission spectrum of a V-type three-level atom due to the interference between the two transitions [11]. However, it has been pointed out by the authors that these effects are found to be significant in a very limited range of atom parameters, that is, the separation of the two upper levels of the atom is required to be comparable with the natural decay rate and thus it is far smaller than the transition frequencies between the lower state and the upper states, which is not a realistic situation in real atoms. It is therefore difficult to experimentally observe such effects with real atoms.

As is known, artificial atoms realizable with superconduction circuits enable the realization of a broad range of light-matter coupling from weak to ultrastrong regimes [22,23]. Reference [24] reports that the interaction between a superconducting qubit and one-dimensional transmission line is so strong that the spontaneous decay rate of the qubit becomes comparable with its transition frequency, in contrast with real atoms. It becomes interesting to explore whether quantum-interference-induced effects such as dark lines and line narrowing exist in the strong-coupling regime and in a wide accessible range of parameters. In addition, counter-rotating couplings which are neglected in the rotating-wave approximation (RWA) become important in the strong-coupling regime. Few efforts have been devoted to studying how those couplings influence the emission spectra of the multilevel emitter in the strong-coupling regime.

In this paper, we study the spontaneous emission spectrum of a V-type artificial atom coupled to a radiation reservoir by using a variational approach and two approximate analytical methods in the strong-coupling regime where the decay rate of the emitter becomes a considerable fraction of its transition frequency. The variational approach is based on the Dirac-Frenkel time-dependent variational principle and the multiple Davydov D_2 (multi-D_2) ansatz [25–27], which goes beyond the RWA and Born-Markovian approximation and is shown to be accurate in certain strong-coupling regimes. One analytical method is based on a unitary transformation [28] which allows us to derive a RWA-like effective Hamiltonian and is named the transformed RWA (TRWA) method; the other analytical method is based on the widely used RWA. By comparing the survival probabilities of the excited state and emission spectra calculated by the three methods, we show that the TRWA method is capable of providing a fairly accurate description of the spontaneous emission of the V-type artificial atom in the strong-coupling regime while the RWA breaks down. We

[*]yiyingyan@zust.edu.cn

illustrate that in the strong-coupling regime significant dark lines and line narrowing can be observed in the emission spectra in a wide range of parameters. Particularly, it is feasible to observe such effects in the case of a relatively large separation of the two upper states of the three-level emitter, which is accessible with artificial atoms in the circuit-QED setups. This paves the way for experimental observation of such phenomena in artificial atoms.

This paper is organized as follows: In Sec. II, we introduce the theoretical model and the methodologies including the time-dependent variational approach, the TRWA, and the RWA. In Sec. III, we compare the survival probabilities of the excited state calculated by the three methods and study the steady-state emission spectra in the strong-coupling regime. In Sec. IV, the conclusions are drawn.

II. MODEL AND METHODOLOGIES

We consider that a V-type artificial atom is strongly coupled to a multimode radiation field, which is described by the Hamiltonian ($\hbar = 1$)

$$H = H_S + H_R + H_I, \tag{1}$$

where

$$H_S = \sum_{j=0}^{2} \Omega_j |j\rangle\langle j|, \tag{2}$$

$$H_R = \sum_k \omega_k b_k^\dagger b_k, \tag{3}$$

$$H_I = \sum_k \frac{\lambda_k}{2} L(b_k + b_k^\dagger). \tag{4}$$

Here, H_S is the free Hamiltonian of a V-type three-level artificial atom, where $|0\rangle$ is the ground state with the energy $\hbar\Omega_0 \equiv 0$, and $|1\rangle$ and $|2\rangle$ are the excited states. $\Omega_j (j = 1, 2)$ is the transition frequency between the excited state $|j\rangle$ and the ground state $|0\rangle$. H_R is the free Hamiltonian of the multimode radiation field. $b_k (b_k^\dagger)$ is the annihilation (creation) operator of the kth bosonic mode with frequency ω_k. H_I is the interaction Hamiltonian between the three-level artificial atom and the reservoir, where λ_k is the coupling constant. $L = L^\dagger$ is the transition operator of the V-type artificial atom and reads

$$L = \sum_{j=1}^{2} r_j(|0\rangle\langle j| + |j\rangle\langle 0|) \equiv \sum_{j=1}^{2} V_j, \tag{5}$$

where r_j is the matrix element for the transition: $|0\rangle \leftrightarrow |j\rangle$.

The dissipation effect of the reservoir is characterized by the Ohmic spectral density

$$J(\omega) = \sum_k \lambda_k^2 \delta(\omega_k - \omega) = 2\alpha\omega\Theta(\omega_c - \omega), \tag{6}$$

where α is the dimensionless coupling constant, $\Theta(\cdot)$ is the Heaviside function, and ω_c is the cutoff frequency. This spectral density is frequently used for the circuit QED [29–31]. For the Ohmic reservoir, when α is close to 0.1, the usual second-order master equation or the RWA is inadequate and a strong-coupling regime is achieved [24,32].

Note that the present model can be physically realized with superconducting circuits [24]. A key feature of such systems

is that their potentials can be manipulated to have a strong anharmonicity. This makes it possible to isolate the few lowest levels from other higher levels [24,33,34]. In this scenario, transitions from the lower-level subspace to the higher-level subspace should be negligible even in the strong-coupling regime. Consequently, a few-level model is still applicable to artificial atoms in the presence of a strong atom-field interaction [22,23].

A. Time-dependent variational approach

In this section, we use the Dirac-Frenkel time-dependent variational principle with the multi-D_2 ansatz to solve the time-dependent Schrödinger equation. To simplify the formal calculation, we use the interaction picture governed by the free Hamiltonian of the reservoir H_R, i.e.,

$$i\frac{d}{dt}|\tilde{\psi}(t)\rangle = \tilde{H}(t)|\tilde{\psi}(t)\rangle, \tag{7}$$

where

$$\tilde{H}(t) = H_S + \sum_k \frac{\lambda_k}{2} L(b_k^\dagger e^{i\omega_k t} + b_k e^{-i\omega_k t}). \tag{8}$$

The Dirac-Frenkel time-dependent variational principle states that with a given trial state $|\tilde{\psi}(t)\rangle$ the optimal solution to the Schrödinger equation can be found via [35]

$$\langle\delta\tilde{\psi}(t)|i\partial_t - \tilde{H}(t)|\tilde{\psi}(t)\rangle = 0, \tag{9}$$

where $\langle\delta\tilde{\psi}(t)|$ is a variation of $\langle\tilde{\psi}(t)|$. In this paper, we use the multi-D_2 ansatz, which is more feasible to treat the "off-diagonal" coupling than the multi-D_1 ansatz (which requires a diagonalized system operator L) [27,36]. The former reads

$$\left|D_2^M(t)\right\rangle = \sum_{n=1}^{M}\sum_{j=0}^{2}(A_{nj}|j\rangle)|f_n\rangle. \tag{10}$$

Here $|f_n\rangle$ is the multimode coherent state,

$$|f_n\rangle = \exp\left[\sum_k(f_{nk}b_k^\dagger - f_{nk}^*b_k)\right]|\mathbf{0}\rangle, \tag{11}$$

where $|\mathbf{0}\rangle$ is the multimode vacuum state of the reservoir. In the trial state, the amplitudes A_{nj} and the displacements f_{nk} are the time-dependent variational parameters.

The equations of motion for the variational parameters can be obtained via Eq. (9) and read

$$i\langle j|\langle f_l|\dot{D}_2^M(t)\rangle = \langle j|\langle f_l|\tilde{H}(t)|D_2^M(t)\rangle, \tag{12}$$

$$i\sum_{j=0}^{2}A_{lj}^*\langle j|\langle f_l|b_k|\dot{D}_2^M(t)\rangle = \sum_{j=0}^{2}A_{lj}^*\langle j|\langle f_l|b_k\tilde{H}(t)|D_2^M(t)\rangle. \tag{13}$$

These equations of motion can be written in a matrix form and be integrated with the fourth-order Runge-Kutta algorithm [26,32]. We present the technique details in Appendix A.

To perform the simulation, we use a finite number of bosonic modes and specify the initial state as follows. The coupling constants λ_k and the frequencies ω_k are obtained by

the linear discretization of the spectral density, that is, they are determined by the following integrals [37]:

$$\lambda_k^2 = \int_{x_{k-1}}^{x_k} J(x)dx, \qquad (14)$$

$$\omega_k = \lambda_k^{-2} \int_{x_{k-1}}^{x_k} xJ(x)dx, \qquad (15)$$

where $x_k = k\omega_c/N_b$ $(k = 0, 1, \ldots, N_b)$ and N_b is the total number of modes. In addition, we should also specify the initial state of the whole system, which is chosen to be a product state $|\Psi(0)\rangle|\mathbf{0}\rangle$, where

$$|\Psi(0)\rangle = \cos\theta|1\rangle + e^{i\varphi}\sin\theta|2\rangle \qquad (16)$$

is the initial state for the V-type artificial atom.

On solving the equations of motion, we can calculate the physical quantities of interest such as the survival probabilities of the interested states and the emission spectrum. For the V-type artificial atom, we mainly calculate the survival probability of the state $|\mathbf{10}\rangle \equiv |1\rangle \otimes |\mathbf{0}\rangle$, which is relevant to the spontaneous emission process and is given by

$$P_{10}(t) = \left|\langle\mathbf{10}|D_2^M(t)\rangle\right|^2$$
$$= \left|\sum_{n=1}^{M} A_{n1} \exp\left(-\frac{1}{2}\sum_k |f_{nk}|^2\right)\right|^2. \qquad (17)$$

This time-dependent quantity will be used as a benchmark for addressing the validity of the analytical approaches developed in the following. For the field dynamics, we calculate photon numbers of each mode at time t, which are obtained as follows:

$$N(\omega_k, t) = \langle D_2^M(t)|b_k^\dagger b_k|D_2^M(t)\rangle$$
$$= \sum_{n,l=1}^{M} \sum_{j=0}^{2} A_{lj}^* f_{lk}^* \mathcal{S}_{ln} A_{nj} f_{nk}, \qquad (18)$$

with

$$\mathcal{S}_{ln} = \langle f_l|f_n\rangle$$
$$= \exp\left\{\sum_k \left[f_{lk}^* f_{nk} - \frac{1}{2}(|f_{lk}|^2 + |f_{nk}|^2)\right]\right\}. \qquad (19)$$

It is evident that $N(\omega_k) \equiv \lim_{t\to\infty} N(\omega_k, t)$ as a function of ω_k is just the steady-state spontaneous emission spectrum.

The accuracy of the variational results is measured by the scaled squared norm of the deviation vector [38]

$$\sigma^2(t) = \frac{\left|[i\partial_t - \tilde{H}(t)]|D_2^M(t)\rangle\right|^2}{\omega_0^2}$$
$$= \frac{\langle D_2^M(t)|\tilde{H}^2(t)|D_2^M(t)\rangle - \langle \dot{D}_2^M(t)|\dot{D}_2^M(t)\rangle}{\omega_0^2}, \quad (20)$$

where $\omega_0 = \min\{\Omega_1, \Omega_2\}$. The detailed calculation of this quantity is presented in Appendix A. Typically, the variational results are numerically accurate as long as $\sigma^2(t) < 10^{-2}$ [32]. More specifically, in the benchmark calculation for the well-known spin-boson model, we find that provided $\sigma^2(t) < 10^{-2}$ the present variational approach is able to yield the accurate results predicted by other methods such as the hierarchical

equations of motion [32] and the quasiadiabatic propagator path integral [25].

B. Unitary transformation

In this section, we analytically calculate the survival probability of the excited state and the steady-state emission spectrum by making use of the unitary transformation [28] and resolvent-operator formalism [39]. The former allows us to go beyond the RWA and the weak-coupling regime while the latter allows us to calculate the transition amplitudes easily.

We begin by transforming the Hamiltonian with a polaron-like unitary transformation [28],

$$H' = e^S H e^{-S},$$
$$= H + [S, H] + \frac{1}{2}[S, [S, H]] + \cdots, \qquad (21)$$

where

$$S = \sum_k \sum_{j=1}^{2} \frac{\lambda_k}{2\omega_k}(b_k^\dagger - b_k)\xi_{k,j}V_j, \qquad (22)$$

with $\xi_{k,j}$ being the parameters to be determined later. By neglecting the higher-order terms, we derive an effective Hamiltonian in the transformed frame

$$H' \approx H_0' + H_1', \qquad (23)$$

where H_0' and H_1' are the free and interaction Hamiltonian, respectively. The free Hamiltonian H_0' is given by

$$H_0' = \sum_{j=0}^{2} \tilde{\Omega}_j|j\rangle\langle j| + \sum_k \omega_k b_k^\dagger b_k, \qquad (24)$$

where

$$\tilde{\Omega}_0 = \sum_{i=1}^{2} \frac{\alpha r_i^2}{2}\left[\Omega_i\left(\ln\frac{\Omega_i + \omega_c}{\Omega_i} - \frac{\omega_c}{\omega_c + \Omega_i}\right) - \frac{\omega_c^2}{\omega_c + \Omega_i}\right], \qquad (25)$$

$$\tilde{\Omega}_j = \Omega_j\left[1 - \frac{\alpha r_j^2}{2}\left(\ln\frac{\Omega_j + \omega_c}{\Omega_j} - \frac{\omega_c}{\omega_c + \Omega_j}\right)\right]$$
$$- \frac{\alpha r_j^2 \omega_c^2}{2(\omega_c + \Omega_j)} \quad (j = 1, 2). \qquad (26)$$

Note that the transition frequencies of the excited states have been renormalized due to the system-reservoir coupling.

The interaction Hamiltonian H_1' reads

$$H_1' = \sum_k \sum_{i=1}^{2} \tilde{\lambda}_{k,i}(b_k^\dagger|0\rangle\langle i| + b_k|i\rangle\langle 0|)$$
$$- W(|1\rangle\langle 2| + |2\rangle\langle 1|), \qquad (27)$$

where

$$\tilde{\lambda}_{k,i} = \frac{r_i \Omega_i \lambda_k}{\omega_k + \Omega_i}, \qquad (28)$$

$$W = \frac{\alpha r_1 r_2}{4} \left\{ 2\omega_c + \frac{1}{\Omega_2 - \Omega_1} \left[3\Omega_1 \Omega_2 \ln \frac{\Omega_1(\Omega_2 + \omega_c)}{\Omega_2(\Omega_1 + \omega_c)} \right. \right.$$
$$\left. \left. + \sum_{j=1}^{2} (-1)^j \Omega_j^2 \ln \frac{\Omega_j + \omega_c}{\Omega_j} \right] \right\}. \quad (29)$$

Clearly, $\tilde{\lambda}_{k,i}$ is the effective coupling constant between the state $|i\rangle$ and the bosonic mode k, and W is the reservoir-induced exchange coupling strength between the two excited states. It is worthwhile to note that the system-field interaction takes the rotating-wave form and the renormalized parameters are responsible for incorporating the effects of the counter-rotating couplings. The present treatment is referred to as the TRWA since we have constructed a RWA-like Hamiltonian in the transformed frame. The detailed derivation of the above effective Hamiltonian is presented in Appendix B.

Although the unitary transformation used resembles the well-known polaron transformation [40–43], there are three differences between them. First, in the transformation generator S, we have introduced parameters $\xi_{k,j}$ and they are determined by requiring the first-order system-reservoir coupling to take the RWA-like form and are found to be less than 1. When $\xi_{k,j} = 1$, the unitary transformation becomes the same as the standard polaron transformation. Second, the operator V_j in the TRWA treatment is not required to be diagonal while it is taken to be diagonal in deriving the polaron-transformed master equation [41–43]. Third, we use the transformation to reformulate the interaction term H_I while the polaron transformation eliminates the interaction term H_I. In addition, we should point out the fact that the standard polaron-transformed master equation is not applicable to the spin-boson model with the Ohmic spectral density due to the infrared divergence; however, a variational master equation may be used to study the present problem [44]. Nevertheless, since we are interested in the spontaneous emission and there are only few states involved in the problem, it is much easier to use the resolvent-operator formalism or wave-function approach than the master-equation approach because the latter captures only the reduced dynamics and should be combined with the quantum regression theory to calculate the emission spectrum [45], which is not as convenient as the resolvent-operator formalism.

We use the effective Hamiltonian and resolvent-operator formalism to calculate the survival probability of the state $|10\rangle$ when the initial state is given by $|\Psi(0)\rangle|\mathbf{0}\rangle$. The survival probability is found to be given by

$$P_{10}(t) = |\langle \mathbf{10}|U(t)|\Psi(0)\rangle|\mathbf{0}\rangle|^2$$
$$\approx \left| \frac{\cos\theta}{\pi} \int_0^{\omega_c} \text{Im} \left[\frac{\tilde{A}_2(\omega)}{\tilde{A}_1(\omega)\tilde{A}_2(\omega) - \tilde{B}^2(\omega)} \right] e^{-i\omega t} d\omega \right.$$
$$\left. + \frac{e^{i\phi}\sin\theta}{\pi} \int_0^{\omega_c} \text{Im} \left[\frac{\tilde{B}(\omega)}{\tilde{A}_1(\omega)\tilde{A}_2(\omega) - \tilde{B}^2(\omega)} \right] e^{-i\omega t} d\omega \right|^2, \quad (30)$$

where $U(t) = \exp(-iHt)$ and

$$\tilde{A}_j(\omega) = \omega - (\tilde{\Omega}_j - \tilde{\Omega}_0) - \tilde{\Delta}_{jj}(\omega) + i\tilde{\Gamma}_{jj}(\omega), \quad (31)$$

$$\tilde{B}(\omega) = -W + \tilde{\Delta}_{12}(\omega) - i\tilde{\Gamma}_{12}(\omega), \quad (32)$$

$$\tilde{\Delta}_{jj}(\omega) = \frac{2\alpha r_j^2 \Omega_j^2}{(\omega + \Omega_j)^2} \left[\omega \ln \left| \frac{\omega(\omega_c + \Omega_j)}{\Omega_j(\omega - \omega_c)} \right| - \omega_c \frac{\omega + \Omega_j}{\omega_c + \Omega_j} \right], \quad (33)$$

$$\tilde{\Gamma}_{jj'}(\omega) = \pi \frac{r_j \Omega_j}{(\omega + \Omega_j)} \frac{r_{j'} \Omega_{j'}}{(\omega + \Omega_{j'})} J(\omega), \quad (34)$$

$$\tilde{\Delta}_{12}(\omega) = \frac{2\alpha r_1 r_2 \Omega_1^2 \Omega_2^2}{(\omega + \Omega_1)(\omega + \Omega_2)(\Omega_2 - \Omega_1)} \left[\ln \frac{\Omega_1(\omega_c + \Omega_2)}{\Omega_2(\omega_c + \Omega_1)} \right.$$
$$\left. + \frac{\omega}{\Omega_1 \Omega_2} \sum_{j=1}^{2} (-1)^j \Omega_j \ln \left| \frac{\omega(\omega_c + \Omega_j)}{\Omega_j(\omega - \omega_c)} \right| \right]. \quad (35)$$

Moreover, the steady-state emission spectrum can be calculated as follows:

$$N(\omega_k) = \lim_{t \to \infty} |\langle 01_k|U(t)|\Psi(0)\rangle|\mathbf{0}\rangle|^2$$
$$\approx \left| \cos\theta \left[\frac{\tilde{\lambda}_{k,1}\tilde{A}_2(\omega_k) + \tilde{\lambda}_{k,2}\tilde{B}(\omega_k)}{\tilde{A}_1(\omega_k)\tilde{A}_2(\omega_k) - \tilde{B}^2(\omega_k)} + \frac{\tilde{\lambda}_{k,1}}{2\Omega_1} \right] \right.$$
$$\left. + e^{i\varphi}\sin\theta \left[\frac{\tilde{\lambda}_{k,1}\tilde{B}(\omega_k) + \tilde{\lambda}_{k,2}\tilde{A}_1(\omega_k)}{\tilde{A}_1(\omega_k)\tilde{A}_2(\omega_k) - \tilde{B}^2(\omega_k)} + \frac{\tilde{\lambda}_{k,2}}{2\Omega_2} \right] \right|^2, \quad (36)$$

where $|01_k\rangle$ represents that the emitter is in the ground state and a photon appears in the kth mode. The detailed derivation of Eqs. (30) and (36) can be found in Appendix C.

The TRWA spectrum (36) is too complicated to offer insights into the spectral features. We acquire a simplification of the TRWA spectrum by using the following approximation:

$$\tilde{A}_j(\omega) \to \omega - (\tilde{\Omega}_j - \tilde{\Omega}_0) - \tilde{\Delta}_{jj} + i\tilde{\Gamma}_{jj} \equiv \omega - \tilde{a}_j, \quad (37)$$

$$\tilde{B}(\omega) \to -W + \tilde{\Delta}_{12} - i\tilde{\Gamma}_{12} \equiv \tilde{b}, \quad (38)$$

where $\tilde{\Delta}_{jj'}$ and $\tilde{\Gamma}_{jj'}$ are the values of $\tilde{\Delta}_{jj'}(\omega)$ and $\tilde{\Gamma}_{jj'}(\omega)$ at $\omega = \overline{\omega}_{12}$, respectively, and $\overline{\omega}_{12} = \frac{1}{2}(\tilde{\Omega}_1 + \tilde{\Omega}_2) - \tilde{\Omega}_0$ is the average transition frequency between the upper levels and the lower level. The above approximation is equivalent to replacing $H_0' + \mathcal{P}R(z)\mathcal{P}$ in Eqs. (C5)–(C8) with $H_0' + \mathcal{P}R(\overline{\omega}_{12} + \tilde{\Omega}_0 + i0^+)\mathcal{P}$, which corresponds to Markovian approximation and can be justified when $\tilde{\Delta}_{jj'}(\omega)$ and $\tilde{\Gamma}_{jj'}(\omega)$ are slowly varying functions of ω [39]. Furthermore, we also neglect the constant terms $1/(2\Omega_j)$ in Eq. (36). In doing so, we obtain a simplified TRWA spectrum

$$N(\omega_k) = |v_k^{(+)}|^2 \frac{1}{|\omega_k - z_+|^2} + |v_k^{(-)}|^2 \frac{1}{|\omega_k - z_-|^2} + 2\text{Re}\left[v_k^{(+)} v_k^{*(-)} \frac{1}{(\omega_k - z_+)(\omega_k - z_-^*)} \right], \quad (39)$$

$$v_k^{(\pm)} = \frac{\pm \cos\theta[\tilde{\lambda}_{k,1}(z_\pm - \tilde{a}_2) + \tilde{\lambda}_{k,2}\tilde{b}] \pm e^{i\varphi}\sin\theta[\tilde{\lambda}_{k,1}\tilde{b} + \tilde{\lambda}_{k,2}(z_\pm - \tilde{a}_1)]}{z_+ - z_-}, \quad (40)$$

where $v_k^{(\pm)}$ are the weight factors, and $z_\pm$ are the solutions of the equation $(z - \tilde{a}_1)(z - \tilde{a}_2) - \tilde{b}^2 = 0$ for the variable z and read

$$z_\pm = \overline{\omega}_{12} + \frac{1}{2}(\tilde{\Delta}_{11} + \tilde{\Delta}_{22}) \mp \sqrt{\rho} \cos\left(\frac{\phi}{2}\right)$$
$$- i\left[\frac{1}{2}(\tilde{\Gamma}_{11} + \tilde{\Gamma}_{22}) \pm \sqrt{\rho} \sin\left(\frac{\phi}{2}\right)\right]. \quad (41)$$

The quantities ρ and ϕ are given by

$$\rho^2 = \left[\tilde{\delta}_{12}^2 + (W - \tilde{\Delta}_{12})^2 - \tilde{\Gamma}_{12}^2 - \frac{1}{4}(\tilde{\Gamma}_{11} - \tilde{\Gamma}_{22})^2\right]^2$$
$$+ [2\tilde{\Gamma}_{12}(W - \tilde{\Delta}_{12}) - \tilde{\delta}_{12}(\tilde{\Gamma}_{11} - \tilde{\Gamma}_{22})]^2, \quad (42)$$

$$\phi = \arctan \frac{2\tilde{\Gamma}_{12}(W - \tilde{\Delta}_{12}) - \tilde{\delta}_{12}(\tilde{\Gamma}_{11} - \tilde{\Gamma}_{22})}{\tilde{\delta}_{12}^2 + (W - \tilde{\Delta}_{12})^2 - \tilde{\Gamma}_{12}^2 - \frac{1}{4}(\tilde{\Gamma}_{11} - \tilde{\Gamma}_{22})^2}, \quad (43)$$

where

$$\tilde{\delta}_{12} = \frac{1}{2}(\tilde{\Omega}_1 - \tilde{\Omega}_2 + \tilde{\Delta}_{11} - \tilde{\Delta}_{22}). \quad (44)$$

We now discuss the physical implications of the simplified TRWA spectrum. It is clear that the first two terms in the spectrum formally contribute to two peaks, the positions and widths of which are determined by the real and imaginary parts of $z_\pm$, respectively. The last term in the simplified TRWA spectrum is the interference term. It turns out that $z_\pm$ play a fundamental role in the formation of the spectrum. The physical significance of $z_\pm$ can be understood by noting that $z_\pm + \tilde{\Omega}_0$ are the eigenvalues of the effective Hamiltonian $H_0' + \mathcal{P}R(\overline{\omega}_{12} + \tilde{\Omega}_0 + i0^+)\mathcal{P}$ of the resolvent operator in the subspace. This suggests that the formation of the spectrum should be understood as a consequence of transitions from two corresponding eigenstates of the effective Hamiltonian in the subspace instead of the two bare upper states to the ground state. The two eigenstates mathematically arise from the superposition of the two bare upper states due to the indirect coupling between them, which is fully captured by the numerator in Eq. (C12). The indirect coupling physically results from the exchange of either real or virtual photons.

C. RWA emission spectrum

To examine the effects of the counter-rotating couplings as well as the improvement of the TRWA over the RWA, we also analytically calculate the survival probability of the excited state and the steady-state emission spectrum with the RWA Hamiltonian, which is obtained by replacing H_I in Eq. (1) with the following one:

$$H_I^{\text{RWA}} = \sum_k \sum_{i=1}^2 \frac{r_i \lambda_k}{2}(b_k^\dagger|0\rangle\langle i| + b_k|i\rangle\langle 0|). \quad (45)$$

By using the RWA Hamiltonian and the resolvent-operator formalism, we derive the survival probability of the state $|10\rangle$,

which is given by

$$P_{10}(t) = \left| \frac{\cos\theta}{\pi} \int_0^{\omega_c} \text{Im}\left[\frac{A_2(\omega)}{A_1(\omega)A_2(\omega) - B^2(\omega)}\right]e^{-i\omega t}d\omega \right.$$
$$\left. + \frac{e^{i\varphi}\sin\theta}{\pi} \int_0^{\omega_c} \text{Im}\left[\frac{B(\omega)}{A_1(\omega)A_2(\omega) - B^2(\omega)}\right]e^{-i\omega t}d\omega \right|^2, \quad (46)$$

where

$$A_j(\omega) = \omega - \Omega_j - r_j^2[\Delta(\omega) - i\Gamma(\omega)], \quad (47)$$

$$B(\omega) = r_1 r_2[\Delta(\omega) - i\Gamma(\omega)], \quad (48)$$

$$\Delta(\omega) = P \sum \frac{\lambda_k^2/4}{\omega - \omega_k} = \frac{\alpha}{2}\left(\omega \ln\left|\frac{\omega}{\omega_c - \omega}\right| - \omega_c\right), \quad (49)$$

$$\Gamma(\omega) = \pi \sum_k \frac{\lambda_k^2}{4}\delta(\omega_k - \omega) = \frac{\pi}{4}J(\omega). \quad (50)$$

The RWA steady-state emission spectrum is

$$N(\omega_k) = \frac{\lambda_k^2}{4}\left| \frac{\cos(\theta)r_1(\omega_k - \Omega_2) + e^{i\varphi}\sin(\theta)r_2(\omega_k - \Omega_1)}{A_1(\omega_k)A_2(\omega_k) - B^2(\omega_k)} \right|^2. \quad (51)$$

It follows from Eq. (51) that $N(\omega_k) = 0$ may occur under certain conditions. For instance, when $\theta = 0$, $N(\omega_k = \Omega_2) = 0$; when $\theta = \pi/2$, $N(\omega_k = \Omega_1) = 0$. In other words, when the V-type artificial atom is initially prepared in one of the excited states, $N(\omega_k)$ becomes zero at the transition frequency of the other excited state [11]. This may result in a dark line in the emission spectrum. It is interesting to examine the influence of the counter-rotating couplings on such dark lines in the strong-coupling regime.

III. DYNAMICS AND STEADY-STATE EMISSION SPECTRA

In this section, we use the aforementioned three methods to calculate the spontaneous emission dynamics and spectrum of the V-type artificial atom in the strong-coupling regime. In numerical calculation, we set the cutoff frequency as $\omega_c = 5\Omega_1$. We will first address the validity of the analytical methods by comparing the survival probabilities of the excited state calculated by the three methods, which also provides insights into the spontaneous emission dynamical process. We then illustrate the dark lines and line narrowing of the emission spectra from the V-type artificial atom in the strong light-matter coupling regime and explore how such phenomena are affected by the counter-rotating couplings, which are expected to have non-negligible effects in the strong-coupling regime.

A. Time evolution of the survival probability of the excited state

We first discuss the validity of the variational multi-D_2 results, which is measured by the deviation $\sigma^2(t)$. It is found that the deviation $\sigma^2(t)$ of the present variational approach with the multi-D_2 ansatz takes on a relatively small magnitude, i.e., $\sigma^2(t) \approx 10^{-3}$, as long as M is large enough and $\alpha \approx 0.1$. More details on the behaviors of $\sigma^2(t)$ with the variation of time are presented in Appendix A. It is therefore reasonable
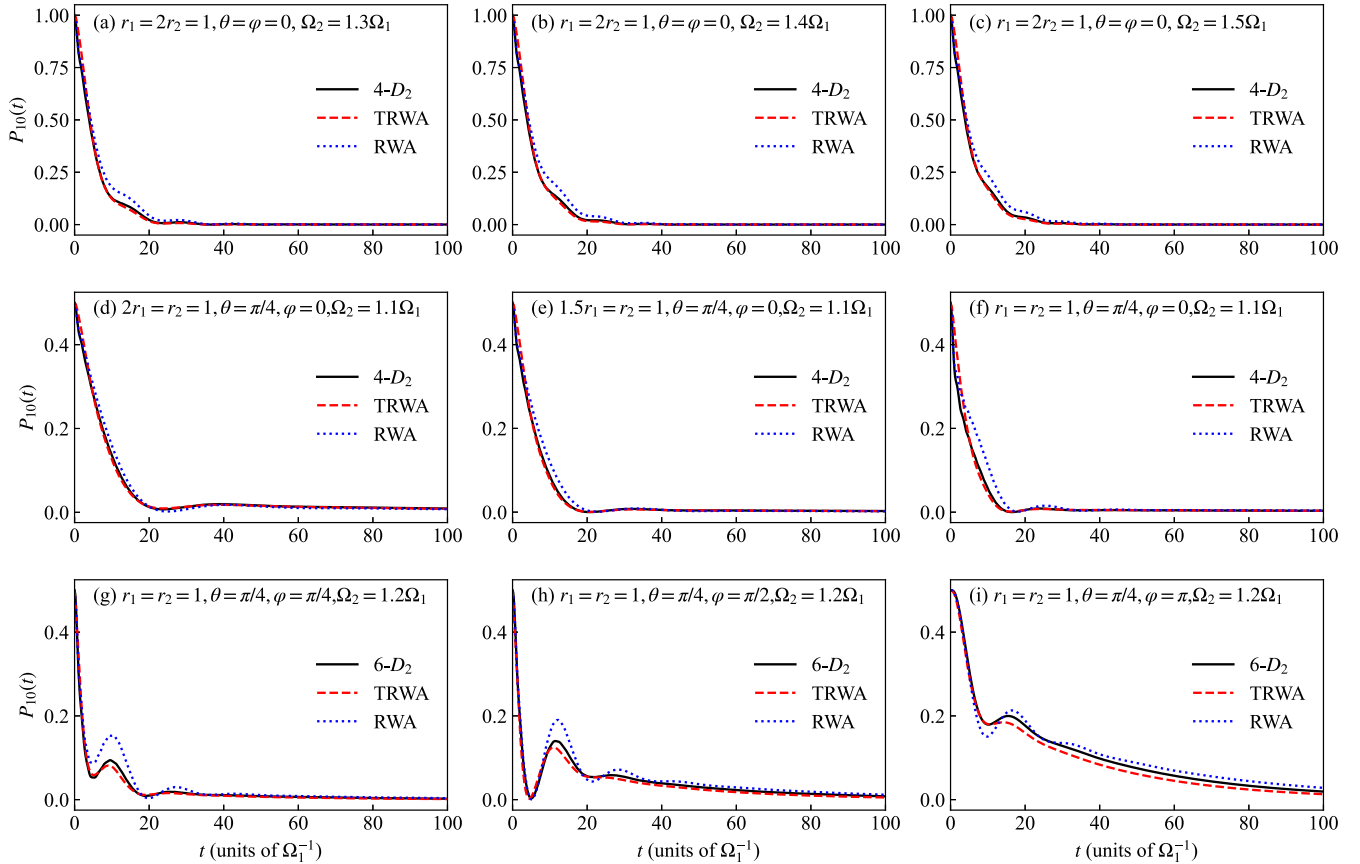
FIG. 1. Survival probability as a function of t calculated by the three methods for $\alpha = 0.05$. The other parameters used are shown in each panel. "4-D_2" represents the variational results with the multiplicity $M = 4$.

to choose the variational results to be the benchmark in this paper. In addition, the convergence of the variational results has been carefully tested by increasing M for fixed N_b and by increasing N_b for fixed M. The number of bath modes used in the numerical simulation is $N_b = 300$. The multiplicity M is shown in the legend of each plot.

Figure 1 shows the survival probability of the excited state $|10\rangle$ as a function of time calculated by the three methods for $\alpha = 0.05$ and various configurations of the other parameters. It is evident that the deviation between the TRWA and the multi-D_2 results is much smaller than that between the RWA and the multi-D_2 results, suggesting that the TRWA has a much better performance than the RWA and the counter-rotating couplings have a non-negligible contribution to the short-time dynamics in the strong-coupling regime. In addition, we should emphasize that in the long-time limit the three methods coincide, that is, the survival probability tends to zero due to the fact that the excited state dies out because of the spontaneous emission.

Figure 2 shows the survival probability of the excited state $|10\rangle$ as a function of time calculated by the three methods for $\alpha = 0.1$ and various configurations of the other parameters. We note that the deviation among the three kinds of results becomes significant for the larger α. Nevertheless, the TRWA provides approximate results with acceptable deviation from the multi-D_2 results. In contrast, the RWA results significantly differ from the multi-D_2 results, suggesting the inadequacy of the RWA.

To summarize, it turns out that the TRWA is applicable to the strong-coupling regime and has a considerable improvement over the RWA when $\alpha \approx 0.1$. On the other hand, Figs. 1 and 2 show that the spontaneous decay of the excited state is not the simple exponential decay, which possesses oscillatory behaviors and can be attributed to the bath-induced exchange interaction between the two upper levels and quantum interference [12]. Moreover, it is worthwhile to note that Figs. 1(i) and 2(i) show that the spontaneous decay of the excited state is relatively slow, indicating that the decay rate is relatively small in spite of the strong system-reservoir coupling and thus the emission spectrum may exhibit a narrow line even in the strong-coupling regime.

B. Dark lines in the emission spectrum

Having compared the short-time evolution of the survival probability of the excited state, we move to study the emission spectra of the V-type artificial atom in the long-time limit. For the variational approach, we propagate the equations of motion for the variational parameters to a final time of $t = 350\Omega_1^{-1}$ and use $N(\omega_k, t)|_{t=350\Omega_1^{-1}}$ to approximate the steady-state emission spectrum. This treatment is found to be sufficient in most cases except for some intractable cases. For instance, in the case of a spectrum exhibiting a significant dark line or line narrowing, the field may need a long time to reach a steady state, which becomes quite numerically demanding. Nevertheless, the quantity $N(\omega_k, t)|_{t=350\Omega_1^{-1}}$ provides a good
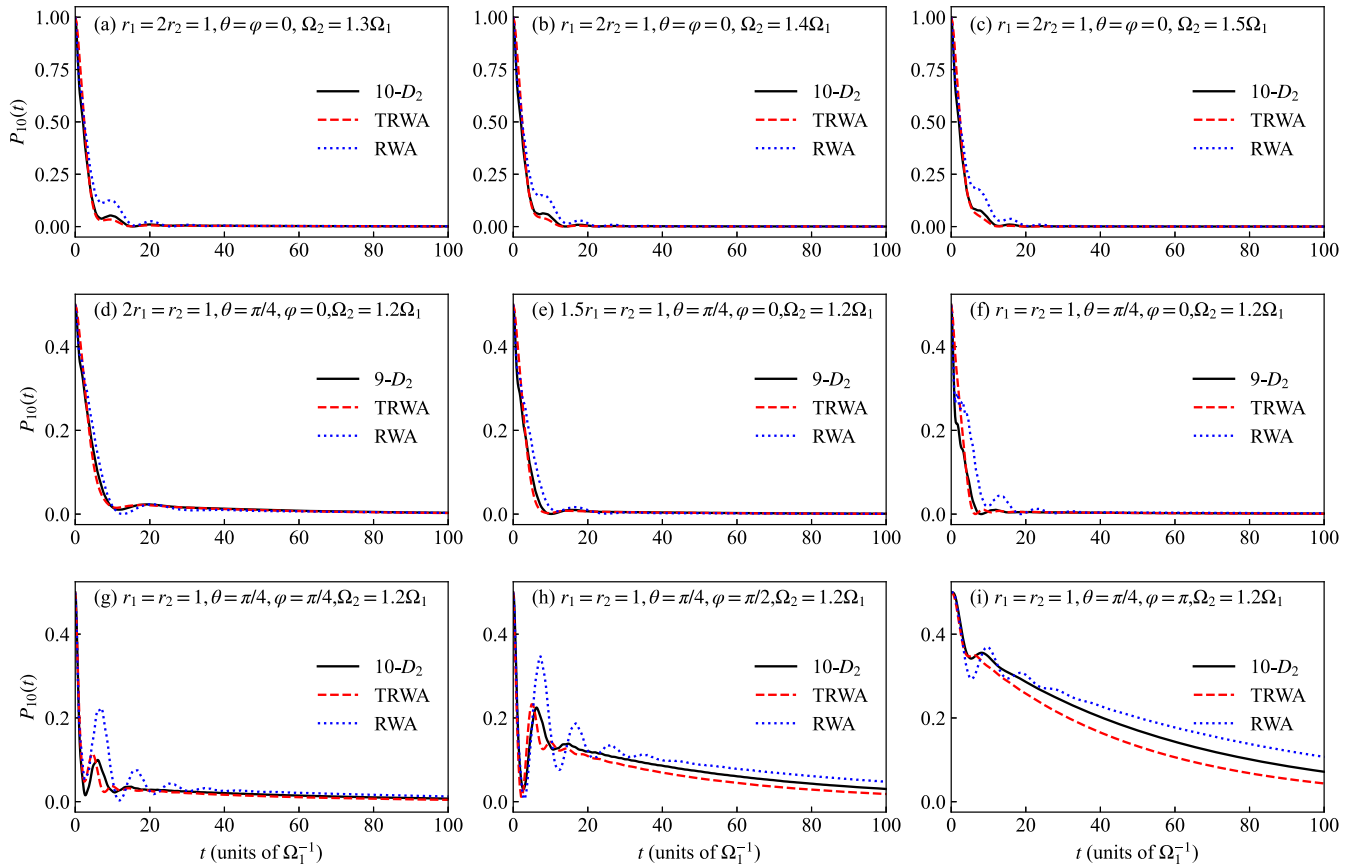
FIG. 2. Survival probability as a function of t calculated by the three methods for $\alpha = 0.1$. The other parameters used are shown in each panel.

approximate description of the steady-state spectrum without essential error.

In Fig. 3, we calculate the steady-state emission spectrum by using the three methods for $\theta = 0$, $\phi = 0$, and $r_1 = 2r_2 = 1$, the two values of α, and the three values of Ω_2. The multi-D_2

spectra and the TRWA spectra agree well with each other, which further confirms the validity of the TRWA. When comparing the RWA spectra with the other ones, we see the two consequences of the RWA on the spectra. One is that the RWA spectra are significantly shifted from the multi-D_2 spectra.
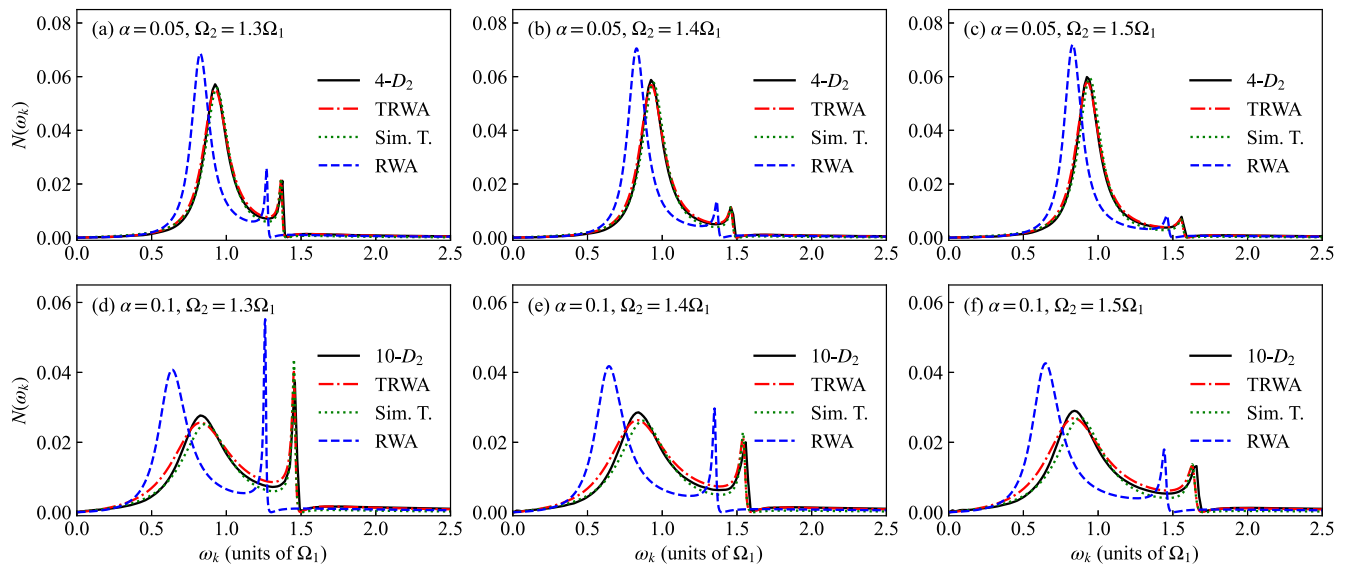
FIG. 3. Emission spectra calculated by the three methods for $r_1 = 2r_2 = 1$ and $\theta = \varphi = 0$. "Sim. T." represents the simplified TRWA spectrum (39). The other parameters used are shown in each panel.
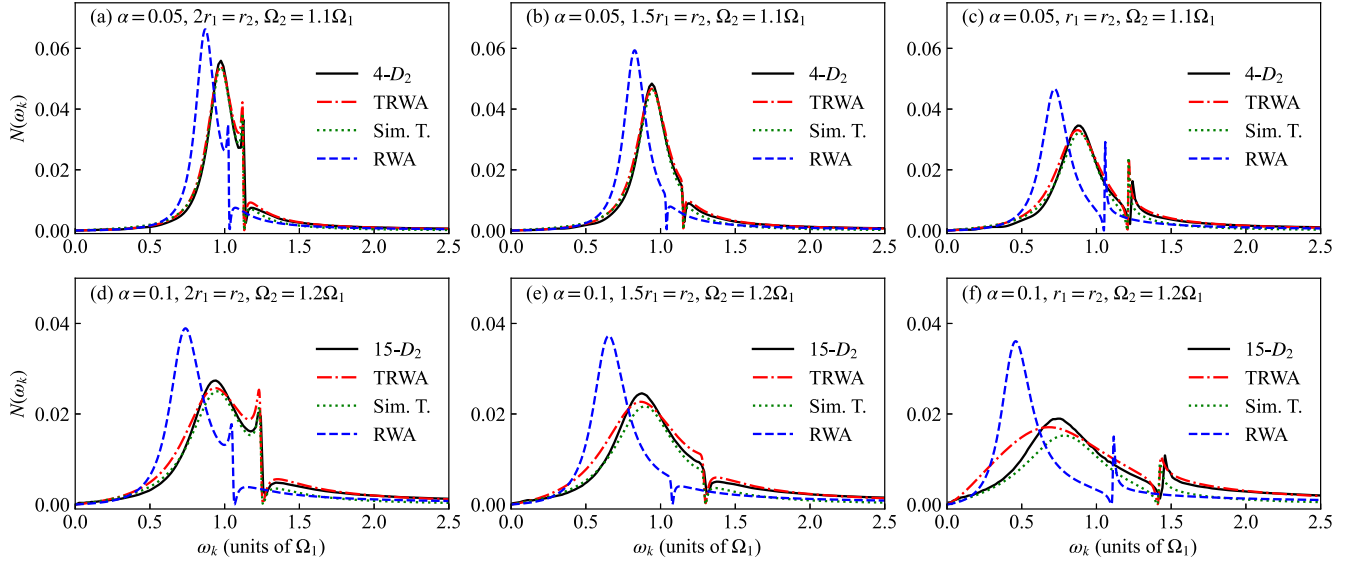
FIG. 4. Emission spectra calculated by the three methods for $r_2 = 1$, $\theta = \pi/4$, and $\varphi = 0$. The other parameters used are shown in each panel.

The other is that the RWA peak is narrower than the multi-D_2 one. This means that the counter-rotating couplings significantly contribute to the peak positions and the linewidths of the spectrum. On the other hand, it is clear to see that the spectra exhibit Fano-type dark lines irrespective of the RWA. More importantly, the present results suggest that the dark line of the V-type artificial atom can be observed in the strong-coupling regime and in the case of a relatively large separation of the two upper levels, i.e., $|\Omega_2 - \Omega_1| \sim \Omega_1$. This is in sharp contrast with the previous work in the weak-coupling regime [11], where the dark lines and line narrowing are found to be significant only in the small separation of the two upper levels, i.e., $|\Omega_2 - \Omega_1| \sim \kappa \ll \Omega_1$ where κ is the spontaneous decay rate of the natural atom.

We now illustrate the dark lines of the emission spectra from the V-type artificial atom when it is initially prepared in the superposition of the two upper states with equal weights, i.e., $\theta = \pi/4$ and $\varphi = 0$. Figures 4(a)–4(c) display the spectra calculated by the three methods for $\alpha = 0.05$, $\Omega_2 = 1.1\Omega_1$, and $r_2 = 1$ and the three values of r_1. The TRWA and multi-D_2 spectra are overall consistent with each other in spite of a discrepancy in the intensities of the dark lines. Such a discrepancy between the TRWA and multi-D_2 spectra can be ascribed to the fact that the latter are obtained at a finite time, i.e., $N(\omega_k, t)|_{t=350\Omega_1^{-1}}$, and they have not reached a steady state for the parameters used in Fig. 4 and can be simply verified by plotting $N(\omega_k, t)$ as a function of time t (the results are not shown here). We will discuss why the variational spectrum does not reach a steady state at $t = 350\Omega_1^{-1}$ under certain conditions in the next section. Nevertheless, the two methods on the existence of dark lines are qualitatively the same. Specifically, when $r_1 = r_2/2$, there exists a Fano-type dark line in the spectrum, which is similar to that found in the weak-coupling regime [11]. As r_1 increases, the dark line profile changes into a dip. When $r_1 = r_2$, the dark line becomes a Fano-type curve again. Figures 4(d)–4(f) display the spectra for $\alpha = 0.1$ and $\Omega_2 = 1.2\Omega_1$, the other parameters being the

same as Figs. 4(a)–4(c), respectively. We see that the profiles of the dark lines in the case of $\alpha = 0.1$ and $\Omega_2 = 1.2\Omega_1$ are similar to those in the case of $\alpha = 0.05$ and $\Omega_2 = 1.1\Omega_1$ except that the dark line broadens.

In Figs. 3 and 4, we see that the simplified TRWA spectrum is qualitatively and acceptably quantitatively correct. Therefore, we can use the simplified TRWA spectrum to further analyze the spectral features due to the quantum-interference effects. It is easy to verify that the dark lines originate from the interference term. To clarify the interference effects that are accessible in a wide parameter regime, in Fig. 5(a), we calculate the interference term in Eq. (39) as a function of ω_k and α for $\Omega_2 = 1.2\Omega_1$, $2r_1 = r_2 = 1$, $\theta = \pi/4$, and $\varphi = 0$; in Fig. 5(b) we calculate the interference term as a function of ω_k and Ω_2 for $\alpha = 0.1$, $2r_1 = r_2 = 1$, $\theta = \pi/4$, and $\varphi = 0$. We see that there are two blue areas where the interference term takes on considerable negative values, indicating a significant modification to the spectrum. The present results suggest that the dark lines may be feasible to be observed in the strong-coupling regime and in the presence of a relatively large separation of the upper levels, which is realizable in superconducting circuit-QED setups.

C. Line narrowing in the emission spectrum

In this section, we illustrate the line narrowing of the V-type artificial atom in the strong-coupling regime. Figure 6 displays the spectra obtained by the three methods for $r_1 = r_2 = 1$, $\Omega_2 = 1.2\Omega_1$, and $\theta = \pi/4$, the two values of α, and the three values of φ. It is evident that the spectrum depends on the relative phase φ of the upper states. Interestingly, there exist a narrow peak and a broad peak in the spectrum. For the special initial state $|\Psi(0)\rangle = (|1\rangle - |2\rangle)/\sqrt{2}$ ($\theta = \pi/4$ and $\varphi = \pi$), the spectrum just exhibits a single narrow peak. In addition, we should point out that the line narrowing can also be illustrated when the V-type artificial atom is initially in one of the upper states for a relatively large separation of the upper levels.
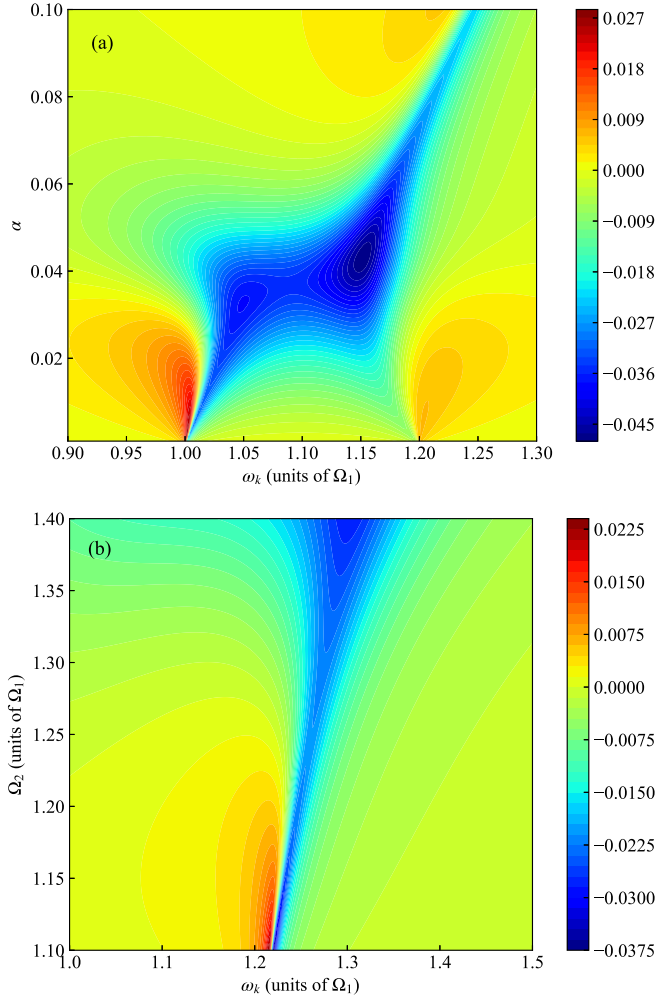
FIG. 5. (a) Interference term in Eq. (39) as a function of ω_k and α for $\Omega_2 = 1.2\Omega_1$. (b) Interference term in Eq. (39) as a function of ω_k and Ω_2 for $\alpha = 0.1$. The other parameters are $2r_1 = r_2 = 1$, $\theta = \pi/4$, and $\varphi = 0$.

Similarly, we use the simplified TRWA spectrum to analyze the origin of the narrow peak as well as the effects of quantum interference on it. To this end, we calculate the emission spectrum and its three components by using the simplified TRWA spectrum (39) for the parameters in Figs. 6(a)–6(c). It can be seen from Fig. 7 that the peak associated with z_- itself has a narrow width and the interference term does not play a fundamental role in the line narrowing. Instead, the interference term may significantly modify the height of the narrow peak. More importantly, in Fig. 7(c), we see that the interference term is weak, and the narrow peak is barely modified by the interference term. We find that a similar situation occurs for $\alpha = 0.1$. This leads us to draw the conclusion that the line narrowing in the strong-coupling regime is due to the behavior of the imaginary part of z_- and fundamentally arises from the photon-mediated interaction between the two upper levels.

A numerical calculation of the real and imaginary parts of $z_\pm$ as a function of α is shown in Fig. 8 for $r_1 = r_2 = 1$ and $\Omega_2 = 1.2\Omega_1$. We find that $|\mathrm{Im}z_+| > |\mathrm{Im}z_-|$ and their deviation increases with α, resulting in a broad and a narrow

peak. Moreover, it is worthwhile to note that the magnitude of $|\mathrm{Im}z_-|$ is on the order of $10^{-2}\Omega_1$ and much smaller than that of $|\mathrm{Im}z_+|$, being on the order of $10^{-1}\Omega_1$ when $\alpha > 0.03$. On the other hand, we note that $\mathrm{Re}z_+ < \mathrm{Re}z_-$, resulting in the broad peak appearing at a lower frequency and the narrow peak appearing at a higher frequency. These findings explain the formation of the spectra shown in Fig. 6 and confirm that the spectrum in the strong-coupling regime should be understood as a consequence of transitions from the two eigenstates of the effective Hamiltonian of the resolvent operator in the subspace to the ground state. The present results suggest that the line narrowing in the emission spectrum of the V-type artificial atom can be observed in a wide accessible range of parameters provided that the system-reservoir coupling is moderately strong. In addition, the small decay rate from z_- is responsible for the fact that the time-dependent spectra obtained by the variational approach do not reach a steady state at $t = 350\Omega_1^{-1}$ since the emitter needs a fairly long time to evolve into a steady state.

IV. CONCLUSIONS

In summary, we have studied the spontaneous emission dynamics and spectrum of the V-type artificial atom in the strong-coupling regime by using the variational approach, TRWA, and RWA. The variational approach combines the Dirac-Frenkel time-dependent variational approach with the multi-D_2 ansatz, which is found to be accurate in the strong-coupling regime. The analytical TRWA method is based on the RWA-like effective Hamiltonian derived from the unitary transformation. The variational approach and TRWA are found to be consistent with each other in predicting short-time dynamics and steady-state emission spectra in the strong-coupling regime, where the RWA breaks down. By using the variational approach and the TRWA, we have shown that the spectrum exhibits significant dark lines and line narrowing in the strong-coupling regime when the separation of the two upper levels is comparable with the transition frequencies of the system, which is accessible in the circuit-QED setup. The dark lines signify the quantum-interference effects. However, the line narrowing is found to be significant even when the quantum-interference effect is weak and physically originates from the photon-mediated interaction between the two upper levels. In addition, we have shown that the counter-rotating couplings have a significant contribution to the peak position and linewidth of the spontaneous emission spectrum in the strong-coupling regime. The present results pave the way for the experimental observation of the quantum-interference-induced effects with artificial atoms in the strong-coupling regime. The present variational approach as well as the TRWA method provide theoretical tools for studying the dynamics, emission spectrum, and quantum interference of the multilevel systems in the strong-coupling regime from the numerical and analytical views, respectively.
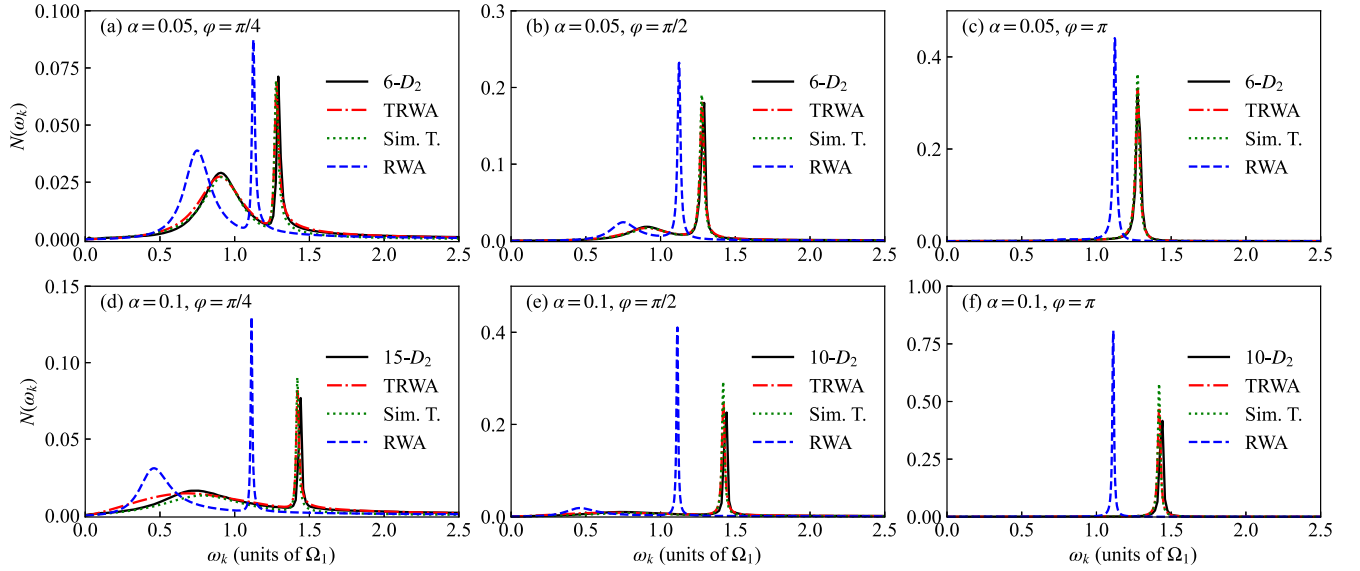
FIG. 6. Emission spectra calculated by the three methods for $r_1 = r_2 = 1$, $\Omega_2 = 1.2\Omega_1$, and $\theta = \pi/4$. The other parameters used are shown in each panel.

APPENDIX A: EQUATIONS OF MOTION FOR THE VARIATIONAL PARAMETERS AND THE SQUARED NORM OF THE DEVIATION VECTOR

One readily differentiates the multi-D_2 state with respect to time t and obtains

$$|\dot{D}_2^M(t)\rangle = \sum_{n=1}^{M}\sum_{j=0}^{2}\left(a_{nj} + A_{nj}\sum_k \dot{f}_{nk}b_k^\dagger\right)|j\rangle|f_n\rangle, \quad (A1)$$

where

$$a_{nj} = \dot{A}_{nj} - A_{nj}\text{Re}\left(\sum_k \dot{f}_{nk}f_{nk}^*\right). \quad (A2)$$

Using Eq. (A1), the explicit forms of the equations of motion can be obtained and further be written in a matrix form,

$$i\begin{pmatrix} \mathcal{S} & & & \mathcal{C}^{(0)} \\ & \mathcal{S} & & \mathcal{C}^{(1)} \\ & & \mathcal{S} & \mathcal{C}^{(2)} \\ \mathcal{C}^{(0)\dagger} & \mathcal{C}^{(1)\dagger} & \mathcal{C}^{(2)\dagger} & \mathcal{G} \end{pmatrix}\begin{pmatrix} \vec{a}_0 \\ \vec{a}_1 \\ \vec{a}_2 \\ \vec{F} \end{pmatrix} = \begin{pmatrix} \vec{I}_0 \\ \vec{I}_1 \\ \vec{I}_2 \\ \vec{I}_F \end{pmatrix}, \quad (A3)$$

where $\mathcal{S}$, $\mathcal{C}^{(j)}$, and $\mathcal{G}$ are $M \times M$, $M \times MN_b$, and $MN_b \times MN_b$ matrices. The elements of these matrices are defined as follows:

$$\mathcal{C}_{l,nk}^{(j)} = A_{nj}\mathcal{S}_{ln}f_{lk}, \quad (A4)$$

$$\mathcal{G}_{lq,nk} = \sum_{j=0}^{2}A_{lj}^*A_{nj}(\delta_{q,k} + f_{lk}^*f_{nq})\mathcal{S}_{ln}, \quad (A5)$$

and $\mathcal{S}_{ln} = \langle f_l|f_n\rangle$. The vectors $\vec{a}_j$ and $\vec{F}$ are defined as follows:

$$\vec{a}_j = (a_{1j}, a_{2j}, \ldots, a_{Mj})^\text{T}, \quad (A6)$$

$$\vec{F} = (\ldots, \dot{f}_{1k}, \dot{f}_{2k}, \ldots, \dot{f}_{Mk}, \ldots)^\text{T}. \quad (A7)$$

The components of the vectors in the inhomogeneous terms in Eq. (A3) read

$$[\vec{I}_j]_l = \langle j|\langle f_l|\tilde{H}(t)|D_2^M(t)\rangle$$
$$= \sum_{n=1}^{M}A_{nj}\Omega_j\mathcal{S}_{ln} + \sum_{n=1}^{M}\sum_{i=0}^{2}A_{ni}\mathcal{S}_{ln}\langle j|L|i\rangle$$
$$\times \sum_k \frac{\lambda_k}{2}(f_{lk}^*e^{i\omega_k t} + f_{nk}e^{-i\omega_k t}), \quad (A8)$$
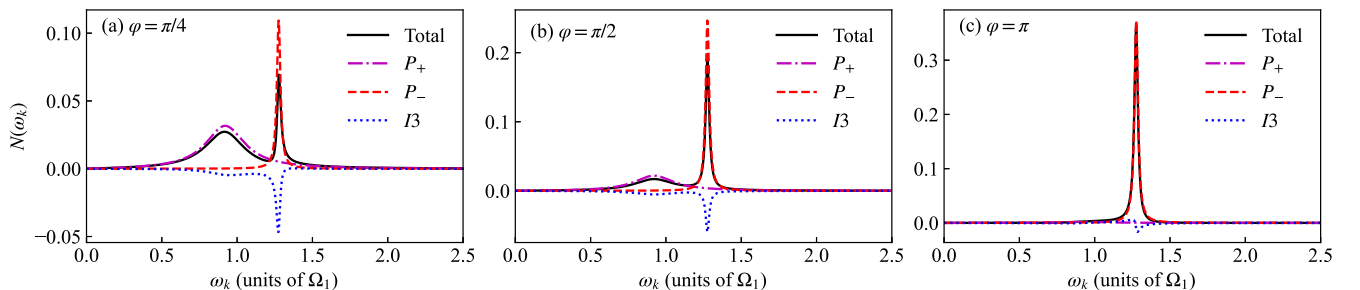

FIG. 7. Emission spectrum and its three components calculated by Eq. (39) for $\alpha = 0.05$, $r_1 = r_2 = 1$, $\theta = \pi/4$, $\Omega_2 = 1.2\Omega_1$, and the three values of φ. "$P_\pm$" and "$I3$" represent the emission lines from the three terms in Eq. (39), respectively. "Total" represents the sum of the three components.

$$[\vec{I}_F]_{lq} = \sum_{j=0}^{2} A_{lj}^* \langle j|\langle f_l|b_q \tilde{H}(t)|D_2^M(t)\rangle$$

$$= \sum_{n=1}^{M}\sum_{j=0}^{2}\left\{\Omega_j A_{lj}^* A_{nj}f_{nq} + \sum_k\sum_{i=0}^{2}\frac{\lambda_k}{2}A_{lj}^*\langle j|L|i\rangle A_{ni}\right.$$

$$\left.\times[\delta_{k,q}e^{i\omega_k t} + (f_{lk}^*e^{i\omega_k t} + f_{nk}e^{-i\omega_k t})f_{nq}]\right\}\mathcal{S}_{ln},\quad \text{(A9)}$$

where $\vec{I}_j$ is an $M \times 1$ vector and $\vec{I}_F$ is arranged as an $MN_b \times 1$ vector.

We state briefly how to numerically integrate the equations of motion. First, one solves the equations of motion as a set of linear equations for the variable vector to obtain the information of the derivatives of the variational parameters. Note that the derivatives of A_{nj} are calculated via Eq. (A2). Second, the obtained derivatives are used to update the variational parameters with the fourth-order Runge-Kutta algorithm. Third, one can repeat the above two steps to obtain the time evolution of the variational parameters.

The scaled squared norm of the deviation vector depends on the mean value of $\tilde{H}^2(t)$ and the squared norm of $|\dot{D}_2^M(t)\rangle$, which can be straightforwardly calculated as follows:

$$\langle \tilde{H}^2(t)\rangle = \langle D_2^M(t)|\tilde{H}^2(t)|D_2^M(t)\rangle$$

$$= \sum_{n,l=1}^{M}\left[\sum_{j=0}^{2}A_{lj}^* A_{nj}\Omega_j^2 + \sum_k\sum_{i=0}^{2}\frac{\lambda_k}{2}A_{lj}^*\langle j|\{H_S,L\}|i\rangle A_{ni}(f_{lk}^*e^{i\omega_k t} + f_{nk}e^{-i\omega_k t})\right]\mathcal{S}_{ln}$$

$$+ \sum_{n,l=1}^{M}\sum_{i,j=0}^{2}A_{lj}^*\langle j|L^2|i\rangle A_{ni}\left\{\left[\sum_k\frac{\lambda_k}{2}(f_{lk}^*e^{i\omega_k t} + f_{nk}e^{-i\omega_k t})\right]^2 + \sum_k\frac{\lambda_k^2}{4}\right\}\mathcal{S}_{ln},\quad \text{(A10)}$$

$$\langle \dot{D}_2^M(t)|\dot{D}_2^M(t)\rangle = (\vec{a}_0^T\ \vec{a}_1^T\ \vec{a}_2^T\ \vec{F}^T)\begin{pmatrix}\mathcal{S} & & & \mathcal{C}^{(0)}\\ & \mathcal{S} & & \mathcal{C}^{(1)}\\ & & \mathcal{S} & \mathcal{C}^{(2)}\\ \mathcal{C}^{(0)\dagger} & \mathcal{C}^{(1)\dagger} & \mathcal{C}^{(2)\dagger} & \mathcal{G}\end{pmatrix}\begin{pmatrix}\vec{a}_0\\ \vec{a}_1\\ \vec{a}_2\\ \vec{F}\end{pmatrix}.\quad \text{(A11)}$$

In Fig. 9, we show the behaviors of $\sigma^2(t)$ as a function of time t for the results shown in Figs. 1 and 2 in the main text. One readily notes that $\sigma^2(t) < 10^{-2}$ is satisfied in each variational result. This suggests that the present variational results are numerically accurate. In addition, we have tried to calculate the deviation in the case of $\alpha = 0.2$ and find that $\sigma^2(t)$ increases to a magnitude of about 0.02 for either $M = 12$ or 14, indicating that the improvement of the ansatz may be needed for a higher accuracy.

APPENDIX B: UNITARY TRANSFORMATION FOR THE V-TYPE ARTIFICIAL ATOM

The unitary transformation can be done as follows:

$$e^S H_S e^{-S} \approx H_S + [S, H_S] + \frac{1}{2}[S,[S,H_S]]$$

$$= H_S + \sum_k\frac{\lambda_k}{2\omega_k}(b_k^\dagger - b_k)$$

$$\times\sum_{i=1}^{2}\xi_{k,i}\Omega_i r_i(|0\rangle\langle i| - |i\rangle\langle 0|)$$

$$- \sum_k\frac{\lambda_k^2}{4\omega_k^2}\left[\sum_{i=1}^{2}r_i^2\xi_{k,i}^2\Omega_i(|i\rangle\langle i| - |0\rangle\langle 0|)\right.$$

$$\left.+ \frac{1}{2}\sum_{i\neq j=1}^{2}r_i r_j\Omega_j\xi_{k,i}\xi_{k,j}(|i\rangle\langle j| + |j\rangle\langle i|)\right]$$

$$+ \sum_{k,p}\frac{\lambda_k\lambda_p}{4\omega_k\omega_p}(b_k^\dagger b_p^\dagger + b_k b_p - b_p^\dagger b_k - b_k^\dagger b_p)$$

$$\times\left[\sum_{i=1}^{2}\xi_{k,i}\xi_{p,i}\Omega_i r_i^2(|i\rangle\langle i| - |0\rangle\langle 0|)\right.$$

$$\left.+ \frac{1}{2}\sum_{i\neq j=1}^{2}r_i r_j\Omega_j(\xi_{k,i}\xi_{p,j}|i\rangle\langle j| + \xi_{p,i}\xi_{k,j}|j\rangle\langle i|)\right],\quad \text{(B1)}$$

$$e^S H_R e^{-S} \approx \sum_k\omega_k b_k^\dagger b_k - \sum_k\frac{\lambda_k}{2}(b_k^\dagger + b_k)\sum_{i=1}^{2}\xi_{k,i}V_i$$

$$+ \sum_k\sum_{i,j=1}^{2}\frac{\lambda_k^2}{4\omega_k}\xi_{k,i}\xi_{k,j}V_i V_j$$

$$- \frac{1}{2}\sum_{k,p}\frac{\lambda_k\lambda_p}{4\omega_p}(b_k^\dagger b_p^\dagger - b_k^\dagger b_p + b_p^\dagger b_k - b_k b_p)$$

$$\times\sum_{i,j=1}^{2}\xi_{k,i}\xi_{p,j}[V_j, V_i],\quad \text{(B2)}$$

$$e^S H_I e^{-S} \approx H_I + [S, H_I]$$

$$= H_I - \sum_k\frac{\lambda_k^2}{4\omega_k}\sum_{i,j=1}^{2}\xi_{k,i}\{V_i, V_j\}$$
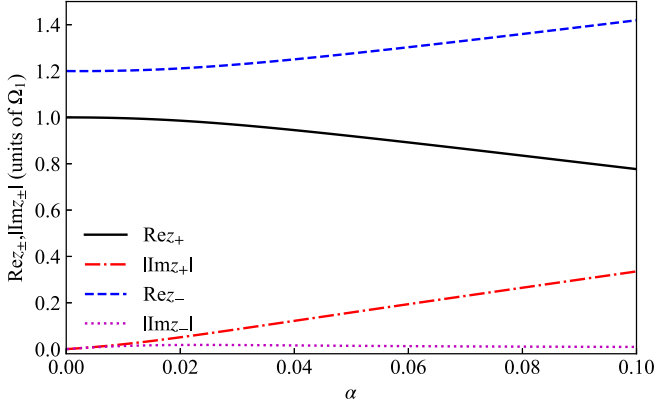
FIG. 8. Real and imaginary parts of $z_\pm$ as a function of α for $r_1 = r_2 = 1$ and $\Omega_2 = 1.2\Omega_1$. The absolute values are taken for the imaginary parts.

$$+ \sum_{k,p} \frac{\lambda_k \lambda_p}{4\omega_k} (b_k^\dagger b_p^\dagger + b_k^\dagger b_p - b_p^\dagger b_k - b_k b_p)$$
$$\times \sum_{i,j=1}^{2} \xi_{k,i}[V_i, V_j]. \quad (B3)$$

We construct the diagonal part of the effective Hamiltonian by collecting the diagonal terms of the decoupled artificial atom and the reservoir in Eqs. (B1)–(B3), which leads to

$$H_0' = \sum_{j=0}^{2} \tilde{\Omega}_j |j\rangle\langle j| + \sum_k \omega_k b_k^\dagger b_k. \quad (B4)$$

The energies of the three states are renormalized and given by

$$\tilde{\Omega}_0 = \sum_{i=1}^{2} \sum_k \left[\frac{\lambda_k^2}{4\omega_k^2} \xi_{k,i}^2 \Omega_i r_i^2 + \frac{\lambda_k^2}{4\omega_k} r_i^2 (\xi_{k,i}^2 - 2\xi_{k,i}) \right], \quad (B5)$$

$$\tilde{\Omega}_j = \Omega_j \left(1 - \sum_k \frac{\lambda_k^2}{4\omega_k^2} \xi_{k,j}^2 r_j^2 \right)$$
$$+ \sum_k \frac{\lambda_k^2}{4\omega_k} r_j^2 (\xi_{k,j}^2 - 2\xi_{k,j}) \quad (j \neq 0). \quad (B6)$$

The parameters $\xi_{k,i}$ can be determined by minimizing the ground-state energy of $\tilde{H}_0$, that is, $\frac{\partial \tilde{\Omega}_0}{\partial \xi_{k,i}} = 0$. This leads to

$$\xi_{k,i} = \frac{\omega_k}{\omega_k + \Omega_i} \ (i = 1, 2). \quad (B7)$$

The interaction Hamiltonian can be constructed by collecting the off-diagonal terms associated with the zeroth- and first-order bosonic processes, that is,

$$H_1' = H_I - \sum_k \frac{\lambda_k}{2} (b_k^\dagger + b_k) \sum_{i=1}^{2} \xi_{k,i} V_i$$
$$+ \sum_k \frac{\lambda_k}{2\omega_k} (b_k^\dagger - b_k) \sum_{i=1}^{2} \xi_{k,i} \Omega_i r_i (|0\rangle\langle i| - |i\rangle\langle 0|)$$
$$- \sum_k \sum_{i \neq j=1}^{2} \frac{\lambda_k^2}{8\omega_k^2} r_i r_j \Omega_j \xi_{k,i} \xi_{k,j} (|i\rangle\langle j| + |j\rangle\langle i|)$$
$$- \sum_k \sum_{i \neq j=1}^{2} \frac{\lambda_k^2}{4\omega_k} \xi_{k,i} \{V_i, V_j\}$$
$$+ \sum_k \sum_{i \neq j=1}^{2} \frac{\lambda_k^2}{4\omega_k} \xi_{k,i} \xi_{k,j} V_i V_j$$
$$= \sum_k \sum_{i=1}^{2} \frac{r_i \Omega_i \lambda_k}{\omega_k + \Omega_i} (b_k^\dagger |0\rangle\langle i| + b_k |i\rangle\langle 0|)$$
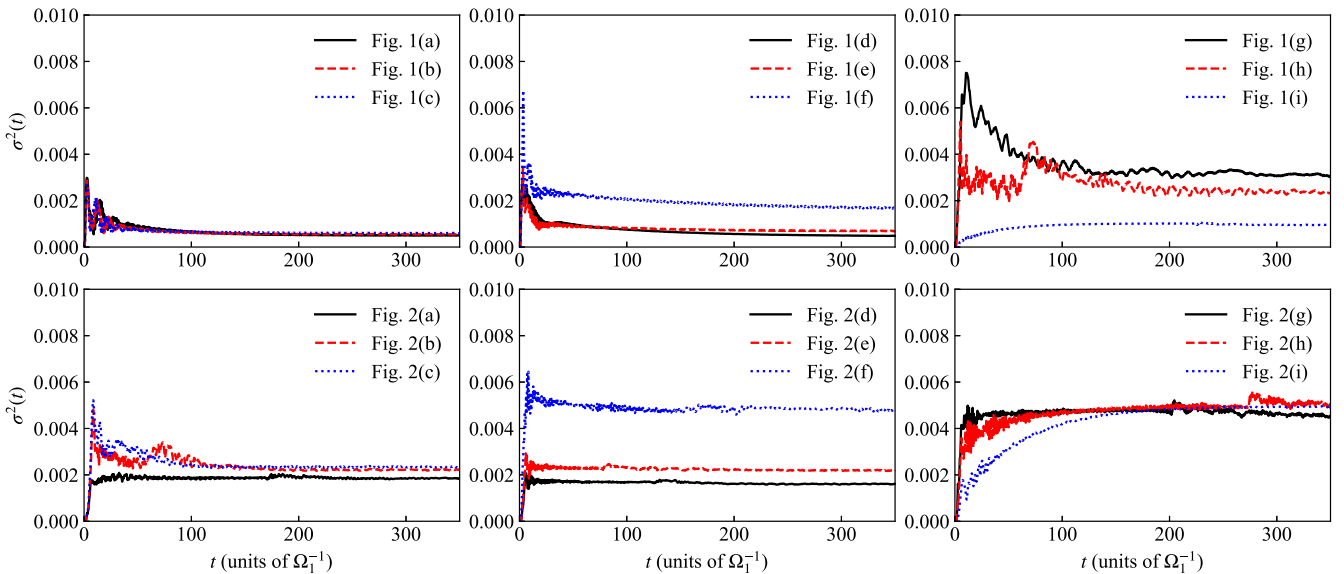$$- W(|1\rangle\langle 2| + |2\rangle\langle 1|), \quad (B8)$$

FIG. 9. Scaled squared norm of the deviation vector $\sigma^2(t)$ as a function of t for the variational results in Figs. 1 and 2 of the main text.

where we have used Eq. (B7) to simplify the system-reservoir interaction terms, and

$$W = \sum_k \frac{\lambda_k^2}{4\omega_k} r_1 r_2 \left[\xi_{k,1}\xi_{k,2} \left(\frac{\Omega_1 + \Omega_2}{2\omega_k} - 1 \right) + \xi_{k,1} + \xi_{k,2} \right].$$
(B9)

APPENDIX C: PROBABILITY AMPLITUDES AND THE RESOLVENT-OPERATOR FORMALISM

Without loss of generality, we show how to use the effective Hamiltonian and resolvent-operator formalism to calculate the probability amplitudes $\langle 10|U(t)|10\rangle$ and $\langle 01_k|U(t)|j0\rangle$ ($j = 1, 2$). It is straightforward to derive the relation between the probability amplitudes in the laboratory frame and those in the transformed frame as follows:

$$\langle 10|U(t)|10\rangle = \langle 10|e^{-S}e^S U(t)e^{-S}e^S|10\rangle$$
$$\approx \langle 10|U'(t)|10\rangle + \sum_q \frac{\tilde{\lambda}_{q,1}}{2\Omega_1} [\langle 01_q|U'(t)|10\rangle$$
$$+ \langle 10|U'(t)|01_q\rangle],$$
(C1)

$$\langle 01_k|U(t)|j0\rangle \approx \langle 01_k|U'(t)|j0\rangle + \sum_q \frac{\tilde{\lambda}_{q,j}}{2\Omega_j} \langle 01_k|U'(t)|01_q\rangle$$
$$- \sum_{i=1}^2 \frac{\tilde{\lambda}_{k,i}}{2\Omega_i} \langle i0|U'(t)|j0\rangle,$$
(C2)

where $\langle 10|U'(t)|10\rangle$ and $\langle 01_q|U'(t)|10\rangle$ are the probability amplitudes in the transformed frame. These quantities can be calculated with the resolvent-operator formalism, which relates the time evolution operator with the resolvent operator via the following integral [39]:

$$U'(t) = \frac{1}{2\pi i} \int_{+\infty}^{-\infty} G(\omega + i0^+)e^{-i\omega t} d\omega,$$
(C3)

where

$$G(z) = \frac{1}{z - H'}$$
(C4)

is the resolvent operator defined with the effective Hamiltonian H' and a complex variable z. To compute the probability amplitudes, we should first calculate the corresponding matrix elements of $G(z)$. To this end, we introduce the projectors $\mathcal{P}$ and $\mathcal{Q}$, where $\mathcal{P} = |10\rangle\langle 10| + |20\rangle\langle 20|$ and $\mathcal{Q} = 1 - \mathcal{P}$. We then use the algebra method to evaluate the projections $\mathcal{P}G(z)\mathcal{P}$, $\mathcal{P}G(z)\mathcal{Q}$, $\mathcal{Q}G(z)\mathcal{P}$, and $\mathcal{Q}G(z)\mathcal{Q}$, which read [39]

$$\mathcal{P}G(z)\mathcal{P} = \frac{\mathcal{P}}{z - H_0' - \mathcal{P}R(z)\mathcal{P}},$$
(C5)

$$\mathcal{Q}G(z)\mathcal{P} = \frac{\mathcal{Q}}{\mathcal{Q}(z - H')\mathcal{Q}} H_1' \frac{\mathcal{P}}{z - H_0' - \mathcal{P}R(z)\mathcal{P}},$$
(C6)

$$\mathcal{P}G(z)\mathcal{Q} = \frac{\mathcal{P}}{z - H_0' - \mathcal{P}R(z)\mathcal{P}} H_1' \frac{\mathcal{Q}}{\mathcal{Q}(z - H')\mathcal{Q}},$$
(C7)

$$\mathcal{Q}G(z)\mathcal{Q} = \frac{\mathcal{Q}}{\mathcal{Q}(z - H')\mathcal{Q}} + \frac{\mathcal{Q}}{\mathcal{Q}(z - H')\mathcal{Q}} H_1'$$
$$\times \frac{\mathcal{P}}{z - H_0' - \mathcal{P}R(z)\mathcal{P}} H_1' \frac{\mathcal{Q}}{\mathcal{Q}(z - H')\mathcal{Q}},$$
(C8)

where

$$R(z) = H_1' + H_1' \frac{\mathcal{Q}}{z - H_0'} H_1' + \cdots$$
(C9)

is the level-shift operator.

The level-shift operator can be computed up to the second order and leads to the matrix elements of $\mathcal{P}G(z)\mathcal{P}$:

$$\langle 20|G(z)|20\rangle = \frac{z - \tilde{\Omega}_1 - \sum_q \frac{\tilde{\lambda}_{q,1}^2}{z - \tilde{\Omega}_0 - \omega_q}}{\tilde{D}(z)},$$
(C10)

$$\langle 10|G(z)|10\rangle = \frac{z - \tilde{\Omega}_2 - \sum_q \frac{\tilde{\lambda}_{q,2}^2}{z - \tilde{\Omega}_0 - \omega_q}}{\tilde{D}(z)},$$
(C11)

$$\langle 20|G(z)|10\rangle = \langle 10|G(z)|20\rangle = \frac{-W + \sum_q \frac{\tilde{\lambda}_{q,1}\tilde{\lambda}_{q,2}}{z - \tilde{\Omega}_0 - \omega_q}}{\tilde{D}(z)},$$
(C12)

where

$$\tilde{D}(z) = \left(z - \tilde{\Omega}_1 - \sum_q \frac{\tilde{\lambda}_{q,1}^2}{z - \tilde{\Omega}_0 - \omega_q} \right)$$
$$\times \left(z - \tilde{\Omega}_2 - \sum_q \frac{\tilde{\lambda}_{q,2}^2}{z - \tilde{\Omega}_0 - \omega_q} \right)$$
$$- \left(W - \sum_q \frac{\tilde{\lambda}_{q,1}\tilde{\lambda}_{q,2}}{z - \tilde{\Omega}_0 - \omega_q} \right)^2.$$
(C13)

By using the above elements, we simply have the following probability amplitudes:

$$\langle 10|U'(t)|10\rangle = \frac{1}{2\pi i} \int_{+\infty}^{-\infty} \langle 10|G(\omega + i0^+)|10\rangle e^{-i\omega t} d\omega$$
$$= \frac{1}{2\pi i} \int_{+\infty}^{-\infty} \frac{\tilde{A}_2(\omega)}{\tilde{A}_1(\omega)\tilde{A}_2(\omega) - \tilde{B}^2(\omega)}$$
$$\times e^{-i(\omega + \tilde{\Omega}_0)t} d\omega$$
$$= -\frac{1}{\pi} \int_0^{\omega_c} \text{Im}\left[\frac{\tilde{A}_2(\omega)}{\tilde{A}_1(\omega)\tilde{A}_2(\omega) - \tilde{B}^2(\omega)} \right]$$
$$\times e^{-i(\omega + \tilde{\Omega}_0)t} d\omega,$$
(C14)

$$\langle 10|U'(t)|20\rangle = \frac{1}{2\pi i} \int_{+\infty}^{-\infty} \langle 10|G(\omega + i0^+)|20\rangle e^{-i\omega t} d\omega$$
$$= \frac{1}{2\pi i} \int_{+\infty}^{-\infty} \frac{\tilde{B}(\omega)}{\tilde{A}_1(\omega)\tilde{A}_2(\omega) - \tilde{B}^2(\omega)}$$
$$\times e^{-i(\omega + \tilde{\Omega}_0)t} d\omega$$
$$= -\frac{1}{\pi} \int_0^{\omega_c} \text{Im}\left[\frac{\tilde{B}(\omega)}{\tilde{A}_1(\omega)\tilde{A}_2(\omega) - \tilde{B}^2(\omega)} \right]$$
$$\times e^{-i(\omega + \tilde{\Omega}_0)t} d\omega,$$
(C15)

where we have used $\frac{1}{x+i0^+} = P\frac{1}{x} - i\pi\delta(x)$ and the Hilbert transform, and we have defined $\tilde{A}_j(\omega)$ and $\tilde{B}(\omega)$ in the main text and the following functions of ω:

$$\tilde{\Delta}_{jj'}(\omega) = P\sum_q \frac{\tilde{\lambda}_{q,j}\tilde{\lambda}_{q,j'}}{\omega - \omega_q}, \tag{C16}$$

$$\tilde{\Gamma}_{jj'}(\omega) = \pi\sum_q \tilde{\lambda}_{q,j}\tilde{\lambda}_{q,j'}\delta(\omega_k - \omega). \tag{C17}$$

It follows from Eqs. (C14) and (C15) that

$$\langle i\mathbf{0}|U'(t)|j\mathbf{0}\rangle \rightarrow 0 \quad (t \rightarrow \infty). \tag{C18}$$

The element $\langle 01_k|G(z)|1\mathbf{0}\rangle$ can be calculated according to Eq. (C6):

$$
\begin{aligned}
\langle 01_k|G(z)|1\mathbf{0}\rangle &= \langle 01_k|\frac{\mathcal{Q}}{\mathcal{Q}(z-H')\mathcal{Q}}H_1'\mathcal{P}G(z)|1\mathbf{0}\rangle \\
&= \sum_q \sum_{i=1}^2 \tilde{\lambda}_{q,i}\langle 01_k|\frac{\mathcal{Q}}{\mathcal{Q}(z-H')\mathcal{Q}}|01_q\rangle \\
&\quad \times \langle i\mathbf{0}|G(z)|1\mathbf{0}\rangle \\
&\approx \sum_{i=1}^2 \frac{\tilde{\lambda}_{k,i}}{z-\tilde{\Omega}_0-\omega_k}\langle i\mathbf{0}|G(z)|1\mathbf{0}\rangle, \tag{C19}
\end{aligned}
$$

where we have used

$$\langle 01_k|\frac{\mathcal{Q}}{\mathcal{Q}(z-H')\mathcal{Q}}|01_q\rangle \approx \frac{1}{z-\tilde{\Omega}_0-\omega_k}\delta_{k,q}. \tag{C20}$$

It follows from Eqs. (C3) and (C19) that

$$
\begin{aligned}
\langle 01_k|U'(t)|1\mathbf{0}\rangle &= \frac{1}{2\pi i}\int_{+\infty}^{-\infty}\langle 01_k|G(\omega+i0^+)|1\mathbf{0}\rangle e^{-i\omega t}d\omega \\
&\approx \frac{1}{2\pi i}\int_{+\infty}^{-\infty}\frac{1}{\omega-\omega_k+i0^+} \\
&\quad \times \frac{\tilde{\lambda}_{k,1}\tilde{A}_2(\omega)+\tilde{\lambda}_{k,2}\tilde{B}(\omega)}{\tilde{A}_1(\omega)\tilde{A}_2(\omega)-\tilde{B}^2(\omega)}e^{-i(\omega+\tilde{\Omega}_0)t}d\omega. \tag{C21}
\end{aligned}
$$

A similar calculation directly leads to

$$
\begin{aligned}
\langle 01_k|U'(t)|2\mathbf{0}\rangle &\approx \frac{1}{2\pi i}\int_{+\infty}^{-\infty}\frac{1}{\omega-\omega_k+i0^+} \\
&\quad \times \frac{\tilde{\lambda}_{k,1}\tilde{B}(\omega)+\tilde{\lambda}_{k,2}\tilde{A}_1(\omega)}{\tilde{A}_1(\omega)\tilde{A}_2(\omega)-\tilde{B}^2(\omega)}e^{-i(\omega+\tilde{\Omega}_0)t}d\omega. \tag{C22}
\end{aligned}
$$

It is clear that the simple pole $\omega = \omega_k - i0^+$ leads to nonvanishing values of the integrals (C21) and (C22) in the long-time limit ($t \rightarrow \infty$). By using the residue theory we simply have the following asymptotic behaviors as $t \rightarrow \infty$:

$$\langle 01_k|U'(t)|1\mathbf{0}\rangle \approx \frac{\tilde{\lambda}_{k,1}\tilde{A}_2(\omega_k)+\tilde{\lambda}_{k,2}\tilde{B}(\omega_k)}{\tilde{A}_1(\omega_k)\tilde{A}_2(\omega_k)-\tilde{B}^2(\omega_k)}e^{-i(\omega_k+\tilde{\Omega}_0)t}, \tag{C23}$$

$$\langle 01_k|U'(t)|2\mathbf{0}\rangle \approx \frac{\tilde{\lambda}_{k,1}\tilde{B}(\omega_k)+\tilde{\lambda}_{k,2}\tilde{A}_1(\omega_k)}{\tilde{A}_1(\omega_k)\tilde{A}_2(\omega_k)-\tilde{B}^2(\omega_k)}e^{-i(\omega_k+\tilde{\Omega}_0)t}. \tag{C24}$$

According to Eq. (C8), we have

$$\langle 01_k|G(z)|01_q\rangle \approx \langle 01_k|\frac{\mathcal{Q}}{\mathcal{Q}(z-H')\mathcal{Q}}|01_q\rangle, \tag{C25}$$

which simply leads to

$$\langle 01_k|U'(t)|01_q\rangle \approx \delta_{k,q}e^{-i(\tilde{\Omega}_0+\omega_k)t}. \tag{C26}$$

With Eqs. (C23)–(C25) at hand, we can obtain the transition amplitude $\langle 01_k|U(t)|j\mathbf{0}\rangle$ ($j = 1, 2$) in the laboratory frame and in the long-time limit according to Eq. (C2):

$$
\begin{aligned}
\langle 01_k|U(t)|1\mathbf{0}\rangle &\approx \left[\frac{\tilde{\lambda}_{k,1}\tilde{A}_2(\omega_k)+\tilde{\lambda}_{k,2}\tilde{B}(\omega_k)}{\tilde{A}_1(\omega_k)\tilde{A}_2(\omega_k)-\tilde{B}^2(\omega_k)}+\frac{\tilde{\lambda}_{k,1}}{2\Omega_1}\right] \\
&\quad \times e^{-i(\omega_k+\tilde{\Omega}_0)t}, \tag{C27}
\end{aligned}
$$

$$
\begin{aligned}
\langle 01_k|U(t)|2\mathbf{0}\rangle &\approx \left[\frac{\tilde{\lambda}_{k,1}\tilde{B}(\omega_k)+\tilde{\lambda}_{k,2}\tilde{A}_1(\omega_k)}{\tilde{A}_1(\omega_k)\tilde{A}_2(\omega_k)-\tilde{B}^2(\omega_k)}+\frac{\tilde{\lambda}_{k,2}}{2\Omega_2}\right] \\
&\quad \times e^{-i(\omega_k+\tilde{\Omega}_0)t}. \tag{C28}
\end{aligned}
$$

Based on the above probability amplitudes, we can easily derive the survival probability (30) and steady-state emission spectrum (36) in the main text.

[1] K.-J. Boller, A. Imamoğlu, and S. E. Harris, Phys. Rev. Lett. **66**, 2593 (1991).

[2] M. Fleischhauer, A. Imamoglu, and J. P. Marangos, Rev. Mod. Phys. **77**, 633 (2005).

[3] D. Roy, Phys. Rev. Lett. **106**, 053601 (2011).

[4] F. Ghafoor and R. G. Nazmitdinov, J. Phys. B **49**, 175502 (2016).

[5] K. McDonnell, L. F. Keary, and J. D. Pritchard, Phys. Rev. Lett. **129**, 200501 (2022).

[6] S.-Y. Zhu and M. O. Scully, Phys. Rev. Lett. **76**, 388 (1996).

[7] M. O. Scully, S.-Y. Zhu, and A. Gavrielides, Phys. Rev. Lett. **62**, 2813 (1989).

[8] B. Schrinski, M. Lamaison, and A. S. Sørensen, Phys. Rev. Lett. **129**, 130502 (2022).

[9] J. Song, C. Li, Y. Xia, Z.-J. Zhang, and Y.-Y. Jiang, J. Phys. B **50**, 175502 (2017).

[10] N. Behzadi, B. Ahansaz, A. Ektesabi, and E. Faizi, Ann. Phys. (NY) **378**, 407 (2017).

[11] S.-Y. Zhu, R. C. F. Chan, and C. P. Lee, Phys. Rev. A **52**, 710 (1995).

[12] S.-Y. Zhu, H. Chen, and H. Huang, Phys. Rev. Lett. **79**, 205 (1997).

[13] J. Jing and T. Yu, Phys. Rev. Lett. **105**, 240403 (2010).

[14] C.-H. Huang, J.-N. Wu, Y.-Y. Li, S.-C. Cheng, and W.-F. Hsieh, Phys. Rev. A **84**, 013802 (2011).

[15] W.-J. Gu and G.-X. Li, Phys. Rev. A **85**, 014101 (2012).

[16] X.-Y. Wang, B.-F. Ding, J.-F. Liu, L. Yan, and H.-P. Zhao, Commun. Theor. Phys. **57**, 276 (2012).

[17] W. Shu, X. Zhao, J. Jing, L.-A. Wu, and T. Yu, J. Phys. B **46**, 175504 (2013).

[18] M. Wiedmann, J. T. Stockburger, and J. Ankerhold, Phys. Rev. A **94**, 052137 (2016).

[19] V. Semin, Laser Phys. **30**, 025204 (2020).

[20] L. Xin, S. Xu, X. X. Yi, and H. Z. Shen, Phys. Rev. A **105**, 053706 (2022).

[21] A. Lee, H. S. Han, F. K. Fatemi, S. L. Rolston, and K. Sinha, Phys. Rev. A **107**, 013701 (2023).

[22] P. Forn-Díaz, L. Lamata, E. Rico, J. Kono, and E. Solano, Rev. Mod. Phys. **91**, 025005 (2019).

[23] A. F. Kockum, A. Miranowicz, S. D. Liberato, S. Savasta, and F. Nori, Nat. Rev. Phys. **1**, 19 (2019).

[24] P. Forn-Díaz, J. J. García-Ripoll, B. Peropadre, J.-L. Orgiazzi, M. A. Yurtalan, R. Belyansky, C. M. Wilson, and A. Lupascu, Nat. Phys. **13**, 39 (2017).

[25] Y. Fujihashi, L. Wang, and Y. Zhao, J. Chem. Phys. **147**, 234107 (2017).

[26] M. Werther and F. Großmann, Phys. Rev. B **101**, 174315 (2020).

[27] Y. Zhao, J. Chem. Phys. **158**, 080901 (2023).

[28] H. Zheng, S. Y. Zhu, and M. S. Zubairy, Phys. Rev. Lett. **101**, 200404 (2008).

[29] G. Díaz-Camacho, A. Bermudez, and J. J. García-Ripoll, Phys. Rev. A **93**, 043843 (2016).

[30] T. Shi, Y. Chang, and J. J. García-Ripoll, Phys. Rev. Lett. **120**, 153602 (2018).

[31] C. A. González-Gutiérrez, J. Román-Roche, and D. Zueco, Phys. Rev. A **104**, 053701 (2021).

[32] Y. Yan, L. Chen, J. Y. Luo, and Y. Zhao, Phys. Rev. A **102**, 023714 (2020).

[33] F. Yoshihara, Y. Nakamura, F. Yan, S. Gustavsson, J. Bylander, W. D. Oliver, and J.-S. Tsai, Phys. Rev. B **89**, 020503(R) (2014).

[34] F. Yoshihara, T. Fuse, S. Ashhab, K. Kakuyanagi, S. Saito, and K. Semba, Nat. Phys. **13**, 44 (2017).

[35] J. Frenkel, *Wave Mechanics* (Oxford University Press, New York, 1934).

[36] M. Werther, F. Grossmann, Z. Huang, and Y. Zhao, J. Chem. Phys. **150**, 234109 (2019).

[37] T. Deng, Y. Yan, L. Chen, and Y. Zhao, J. Chem. Phys. **144**, 144102 (2016).

[38] R. Martinazzo and I. Burghardt, Phys. Rev. Lett. **124**, 150601 (2020).

[39] C. Cohen-Tannoudji, J. Dupont-Roc, and G. Grynberg, *Atom-Photon Interactions: Basic Processes and Applications* (Wiley, New York, 2004).

[40] G. D. Mahan, *Many-Particle Physics* (Plenum, New York, 1990).

[41] D. P. S. McCutcheon and A. Nazir, New J. Phys. **12**, 113042 (2010).

[42] A. Kolli, A. Nazir, and A. Olaya-Castro, J. Chem. Phys. **135**, 154112 (2011).

[43] S. J. Jang, J. Chem. Phys. **157**, 104107 (2022).

[44] F. A. Pollock, D. P. S. McCutcheon, B. W. Lovett, E. M. Gauger, and A. Nazir, New J. Phys. **15**, 075018 (2013).

[45] H.-P. Breuer and F. Petruccione, *The Theory of Open Quantum Systems* (Oxford University Press, New York, 2007).